TWO PHOTOBIOELECTROCHEMICAL APPLICATIONS OF SELF-ASSEMBLED FILMS ON MERCURY

Francesco TADINI BUONINSEGNI[1], Andrea DOLFI[2] and Rolando GUIDELLI[3,*]

Department of Chemistry, Florence University, Via della Lastruccia 3, 50019 Sesto Fiorentino (Firenze), Italy; e-mail: [1] francesco.tadini@unifi.it, [2] andrea.dolfi@unifi.it, [3] guidelli@unifi.it

Received May 20, 2003
Accepted December 8, 2003

Dedicated to Professor Sergio Roffia in honor of his retirement.

The homogeneous, defect-free surface of a hanging mercury drop electrode was used to self-assemble films apt for the investigation of two photobioelectrochemical systems. Monolayers of straight-chain C_{12}–C_{18} alkane-1-thiols were anchored to a hanging mercury drop electrode and a film of chlorophyll was self-assembled on the top of them. The dependence of the photocurrents generated by illumination of the chlorophyll film with red light, on the thickness of the alkane-1-thiol monolayer and the applied potential is discussed. The photocurrents of purple membrane fragments, adsorbed on a mixed hexadecane-1-thiol/dioleoylphosphatidylcholine bilayer self-assembled on mercury, were investigated in the presence of sodium perchlorate, chloride and acetate. The effect of the anions on the kinetics of the light-driven proton transport by bacteriorhodopsin has been determined.
Keywords: Photobioelectrochemistry; Photochemistry; Electrochemistry; Chlorophyll; Bacteriorhodopsin; Alkanethiol monolayers; Mercury-supported films.

Mercury has a homogeneous, featureless, defect-free surface that lends itself to the formation of well-behaved self-assembled monolayers. This is an indisputable advantage of Hg over solid electrodes such as gold, whose surface steps and kinks are responsible for defects in the deposited films. Moreover, mercury electrodes are readily renewable and do not require conditioning prior to use. These advantageous features of Hg have been exploited to investigate the behavior of phospholipid monolayers self-assembled on Hg electrodes and incorporating biomolecules. Thus, these monolayers have been used to incorporate several lipophilic molecules, such as ubiquinone-10 (refs[1,2]), vitamin K_1 (ref.[3]), gramicidin[4,5], prothrombin[6], apolipoprotein A-I (ref.[7]), *etc.*, and to investigate their electrochemical behavior. Hg-supported phospholipid monolayers have hydrocarbon tails directed to-

ward the hydrophobic mercury surface and the polar heads directed toward the aqueous phase; they can be regarded as convenient biomimetic membranes. In fact, the interface between aqueous phase and the polar head region of lipid monolayers is equivalent to that between the same aqueous phase and lipid bilayers that are the main constituents of biological membranes. Thus, as long as interactions with foreign molecules are confined only to the polar head region, no appreciable differences are expected. However, integral proteins span the lipid bilayer of biomembranes completely, often protruding outside the bilayer. Therefore, they cannot be investigated in a functionally active state on metal-supported phospholipid monolayers. Bamberg, Fendler *et al.*[8–11] adopted an ingenious approach that consists of adsorbing membrane fragments or proteoliposomes on a phospholipid monolayer self-assembled on the top of a long-chain alkane-1-thiol monolayer firmly tethered to a gold electrode. In our laboratory, this approach has been conveniently extended to mercury[12–14] sharing with gold a high affinity to thiols and providing a defect-free surface for the thiol monolayer[15].

In this work, two applications of self-assembled films on mercury electrodes related to problems of photobioelectrochemical interest will be described: (i) the dependence of the photocurrents of a chlorophyll (Chl) film self-assembled on the top of alkane-1-thiol monolayers of different chain lengths tethered to a mercury electrode on the thickness of the thiol monolayer and on the applied potential; (ii) the influence of three different anions on the pumping activity of the light-driven proton pump bacteriorhodopsin (bR) present in purple membrane fragments adsorbed on a mixed hexadecane-1-thiol/dioleoylphosphatidylcholine bilayer.

EXPERIMENTAL

Chemicals

The water used was obtained from distilled light mineral water, followed by distillation from alkaline permanganate, while discarding the heads. Reagent-grade KCl (Merck) was baked at 500 °C before use to remove any organic impurities. All inorganic salts were purchased from Merck. Dioleoylphosphatidylcholine (DOPC) from Lipid Products (South Nutfield, Surrey, U.K.) and alkane-1-thiols (Fluka) were used without further purification. The aqueous solutions of pH 8.5, used in Chl photocurrent measurements, were buffered with 5×10^{-3} M H_3BO_3 and 1.2×10^{-3} M NaOH. The solutions of pH 7, used in bR photocurrent measurements, were buffered with 3×10^{-2} M HEPES. Chlorophyll was extracted from the cyanobacterium *Spirulina gelteri* and purified by the method described in ref.[16]. Purple membrane (PM) fragments, prepared by the standard protocol[17], were kindly provided by the Max

Planck Institute for Biophysics (Frankfurt/Main). The stock suspension of PM was prepared by diluting a PM suspension (OD_{568} = 30) ten times with water or with aqueous 1×10^{-1} M KCl.

Experimental Set-Up and Procedures

The experimental set-up employed in the photocurrent measurements of Chl and bR is shown in Fig. 1. The whole set-up was placed in a water-jacketed box D, thermostatted at 25 ± 0.1 °C. The electrolyte solutions in the cells A and C were deaerated by purging with a high-purity argon for at least 20 min. The home-made hanging mercury drop electrode (HMDE) used in the measurements has been described elsewhere[18,19]. In the present measurements, a surface area of 1.4×10^{-2} cm^2 was used. The HMDE was housed in a water-jacketed sleeve on the top of the box so as to permit effective thermostatting of the mercury reservoir. The vertical movements of the HMDE through the argon/solution interface were realized by means of an oleodynamic system; this ensured complete absence of vibrations while permitting an appreciable range of velocities. A second oleodynamic system was used for horizontal movements of the movable support S, on which the two cells A and C and vessel B were placed; this permitted the HMDE to be positioned above, and then lowered into any of these vessels. The water-jacketed box was contained in Faraday cage F to avoid electrical noise. A vibration-free table was also employed to prevent mechanical vibrations.

In the photocurrent measurements of bR, the glass cell A was used to deposit a DOPC monolayer on the top of a hexadecane-1-thiol-coated HMDE. In the photocurrent measurements of both bR and Chl, it was also used to measure the differential capacity of a coated mercury electrode; it contained a platinum counter electrode, a SCE reference electrode and, where required, the HMDE. In the Chl measurements, vessel B contained a Chl solution in a 50% (v/v) ethanol–water mixture, and was used to coat an alkanethiol-coated HMDE with a Chl film (see below). In the bR measurements, it contained a hexadecane-1-thiol (HDT) so-

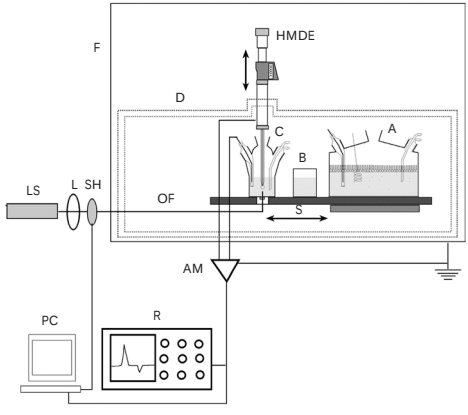

FIG. 1
Experimental set-up. F, Faraday cage; D, water-jacketed box; HMDE, hanging mercury drop electrode; A, three-electrode electrolysis cell; B, vessel; C, two-electrode cell; S, movable support; LS, light source; L, optical fiber coupler; SH, shutter; OF, optical fiber; AM, current amplifier; R, recorder; PC, personal computer

lution in chloroform, when used to self-assemble an HDT monolayer on a bare HMDE (see below), or else an aqueous dispersion of PM fragments, when used to adsorb these fragments on an HMDE coated with an HDT/DOPC mixed bilayer. The methacrylate glass cell C contained a Ag|AgCl (1×10^{-1} M KCl) reference electrode and, where required, the HMDE. It was provided with a quartz optical fiber (0.6 mm diameter), whose tip was positioned on the cell bottom, pointing vertically towards the HMDE for its illumination. For a good alignment of the optical fiber with the mercury drop, the cell was mounted on a *x–y* slide. The monochromatic light source LS (red light laser, 670 nm, Electron, Model LA5-3.5G-670 for Chl measurements; He-Ne laser, 543.5 nm, Uniphase, model 1675 for bR measurements) was focused and collimated, using an optical fiber coupler L (Model F-915T, Newport). Light pulses were produced using an electromechanical shutter SH (blade shutter and digital shutter controller, Model 845, Newport) that was controlled by a PC through a digital-to-analog converter (IOtech Inc. DAC488/2). The current, generated by illuminating either the Chl film or the PM fragments adsorbed on the HMDE under potentiostatic conditions, was amplified (current amplifier, Keithley 428), recorded (16-bit analog-to-digital converter, IOtech Inc. ADC488/8SA), visualized (oscilloscope, Tektronix TDS 340A) and stored (Power PC G3, Macintosh). Operation of the experimental set-up and data acquisition were carried out under computer control (GBIP interface, National Instruments board), using a home-made acquisition program written in LabView environment. To increase the signal-to-noise ratio, current *versus* time curves were stored upon averaging no less than 50 current signals. The signal was usually sampled at 200 μs intervals.

The differential capacitance C and resistance R of alkanethiol-coated mercury were measured by impedance spectroscopy with a Stanford Research SR850 lock-in amplifier upon representing the alkanethiol monolayer as a RC mesh. All potentials are referred to the Ag|AgCl (1×10^{-1} M KCl) reference electrode unless stated otherwise.

Films of Chl were transferred onto an alkanethiol-coated HMDE by immersing it in a solution of Chl in a 50% (v/v) ethanol–water mixture for 15–20 min. The Chl-coated mercury drop was then immersed into the electrolytic solution. Because of the high sensitivity of Chl to the blue and red components of visible light, all measurements were carried out under green light conditions. Self-assembly, characterization and properties of mixed alkanethiol/lipid bilayers supported by mercury are described in ref.[20] The procedure adopted produces a lipid monolayer on the top of the thiol monolayer, with hydrocarbon tails of the two monolayers directed towards each other and polar heads of the lipid monolayer oriented to the solution.

RESULTS AND DISCUSSION

Chlorophyll Films on Alkanethiol-Coated Hg

Chlorophyll is a pigment present in the thylakoid membrane of higher plants, playing a fundamental role in the photosynthesis, whereby solar energy is converted into the stored energy of saccharides. It consists of a porphyrin ring that chelates Mg(II) and contains a network of conjugated double bonds absorbing light. Its long hydrocabon side chain imparts to Chl a high affinity to lipids. In the thylakoid membrane Chl is present in

an antenna complex consisting of hundreds of chlorophyll molecules that absorb light and transfer their energy to a special pair of Chl molecules. These in turn transfer the excited electron to plastoquinone, which is reduced to the corresponding quinol and shuttles electrons to another protein incorporated in the thylakoid membrane. In the excited state, Chl is a strong reductant, with a redox potential of about –1 V *vs* NHE, when it releases the excited electron. It is also a strong oxidant, with a redox potential of about +1 V *vs* NHE, when it takes up an electron to fill the hole left by the excited electron.

In two previous papers[21,22] it was shown that a Chl film self-assembled directly on mercury from an 8×10^{-4} M Chl solution in hexane, once illuminated with red light in an aqueous 1×10^{-1} M KCl solution of pH 8.5, yields a photocurrent that depends notably on the applied potential. Thus, at –0.160 V *vs* SCE, the light-on current is negative, corresponding to a flow of negative charges from the electrode to the solution. Proceeding towards more negative applied potentials, the light-on current first increases, attaining a maximum value at about –0.46 V *vs* SCE. Then it decreases with a further negative shift of the applied potential. Finally, near –0.76 V *vs* SCE, the light-on current starts passing from negative to positive values. The shape of the light-on current suggests the superposition of negative and positive contributions, with the latter prevailing over the former as the applied potential becomes more negative and the illumination time increases. This photoelectrochemical behavior, combined with chronocoulometric measurements of the Chl electroreduction in the dark, was interpreted by assuming that, at more positive potentials, a film of adsorbed Chl dimers mediates electron transfer from the electrode to water. Near –0.8 V *vs* SCE, an incipient Chl electroreduction causes cleavage of the hydrogen bond between the Chl units of the dimers and reorientation of the resulting units. Such a reorientation seems to favor electron transfer from the corresponding photoexcited Chl molecules to the metal rather than to water. The resulting Chl^+ cations can then oxidize water upon oxygen evolution, a process that proceeds with a decrease in Gibbs energy.

In this work we have investigated the photocurrents obtained by illuminating a Chl film deposited on the top of monolayers of alkane-1-thiols with chain lengths ranging from C_{12} to C_{18}, anchored to a mercury electrode. The study was aimed to verify the effect of the potential energy barrier created by these monolayers of different thickness on the transfer of the Chl photoexited electron. Figure 2 shows a series of negative photocurrents obtained on (*n*-C_{14}SH)-coated mercury at different applied potentials over the potential range in which Chl is electroinactive in the dark.

The light-on current attains an almost stationary value in about 0.1 s, while the corresponding light-off current decays exponentially to zero in about the same time. Also here, the negative light-on current is due to the electroreduction of the photoexcited Chl molecule, Chl*, to the corresponding radical anion, Chl^{-}, that transfers its electron to water upon hydrogen evolution, thus sustaining the light-on current. Figure 3 shows plots of the stationary light-on current density I on (n-$C_{12}SH$)- and (n-$C_{14}SH$)-coated mercury, with Chl molecules on the top, as a function of the applied potential E. The slope of these I *vs* E curves tends to decrease slightly at the most negative potentials. This behavior cannot be ascribed to diffusion phenomena, since the current is induced by the photoexitation of Chl molecules, that are insoluble in water and are only present in the adsorbed state. In other words, I is a direct measure of the rate constant k_{app} for the electrode process $Chl^* + e \rightarrow Chl^{-}$:

$$I = Fk_{app}\,\Gamma_{Chl^*}\,, \qquad (1)$$

where Γ_{Chl^*} is the surface concentration of Chl*. The decrease in slope of the curves in Fig. 3 is due to the fact that the driving force $e\eta$, where η is the overpotential and e is the negative electron charge, tends to approach and, ultimately, to exceed the reorganization energy λ for the electrode pro-

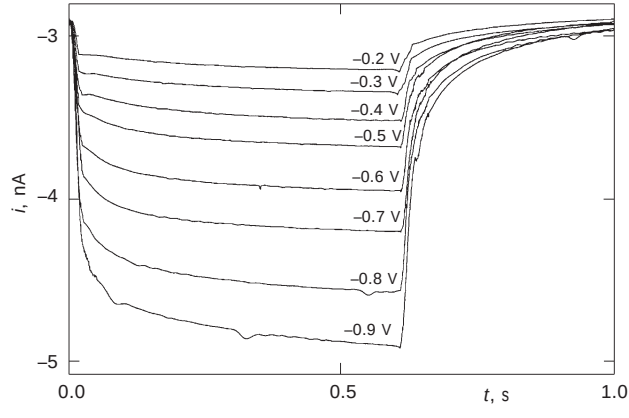

FIG. 2

Light-on and light-off currents recorded upon illuminating a Chl film self-assembled on the top of an n-$C_{14}SH$-coated HMDE in aqueous 1×10^{-1} M KCl (pH 8.5) with red light for 0.6 s at the indicated potentials. The potentials are referred to the Ag|AgCl (1×10^{-1} M KCl) reference electrode. Measurements were carried out on the same freshly prepared drop, starting from the most positive potential and waiting for the stabilization of the background current before illuminating the drop at each potential

cess. In other words, the overlap between the density of the electronic states in the metal and the population of photoexcited Chl molecules tends to a maximum limiting value. As distinct from homogeneous electron transfer reactions, such an overlap cannot decrease when the driving force exceeds λ, giving rise to the Marcus inverted region. This is simply because tunneling from the electronic states in the metal below the Fermi level takes place even when eη exceeds λ.

For a nonadiabatic process, if the Fermi distribution is approximated by a step funtion and the electronic coupling between the redox species and the electrode surface is regarded as independent of the applied potential, the potential dependence of the $dk_{app}/d\eta$ is then expressed by the proportionality relation:

$$dk_{app}/d\eta \propto \exp\left[-(\lambda - e\eta)^2/4\lambda kT\right] . \qquad (2)$$

According to this relationship, the plot of $dk_{app}/d\eta$ *vs* η is a Gaussian, whose maximum value is attained for eη = λ; the slope of the two branches of the Gaussian decreases with increasing λ. Plots of d*I*/d*E* values against *E*, obtained by differentiating the *I vs E* curves in Fig. 3, are shown in Fig. 4. These plots show a maximum that allows an estimate of λ, provided the redox potential, E^0, of the Chl*/Chl^- couple is known. This depends on whether the photoexcited Chl* molecule is in the triplet or singlet state. The redox potentials of the Chl*/Chl^- couple for the triplet and singlet state are approximately equal to +0.2 and +0.7 V *vs* Ag|AgCl (1×10^{-1} M KCl). The

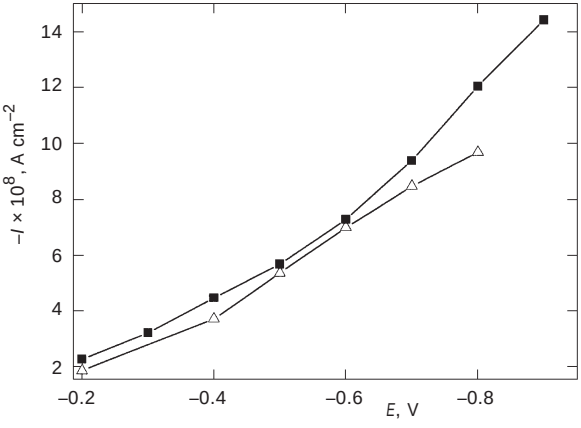

FIG. 3

Plots of the stationary light-on current density *I* on *n*-C_{12}SH- (△) and *n*-C_{14}SH-coated mercury (■), with Chl molecules on the top, as a function of the applied potential *E*

dI/dE *vs* E plots in Fig. 4 were fitted to the expression $A + B \exp[-(\lambda - e\eta)^2/4\lambda kT]$, where the constant term A accounts for the capacitive contribution to the current, and the preexponential factor B includes, among others, the surface concentration of Chl molecules. The latter is not entirely reproducible in passing from a coated electrode to another. By far the best fit, reported in Fig. 4, was obtained by using the redox potential for the triplet state of Chl*. This leads to a reorganization energy λ of about 1.0 eV on (n-C_{14}SH)-coated mercury and of 0.76 eV on (n-C_{12}SH)-coated mercury. These values are in a good agreement with previous electrochemical measurements[23,24] and with Marcus dielectric continuum model for aqueous environment[25].

An abrupt decrease in the stationary light-on photocurrent of more than one order of magnitude is observed on passing from a mercury-supported n-C_{14}SH monolayer to a n-C_{16}SH monolayer, as shown in Fig. 5. The shape of the photocurrent transients is also different in that the current exhibits a sharp peak before decaying to a constant and almost potential-independent stationary value. The light-on photocurrents on (n-C_{18}SH)-coated mercury are similar to those on (n-C_{16}SH)-coated mercury, albeit slightly lower. The abrupt change in the photocurrent behavior from that in Fig. 2 to that in Fig. 5 on passing from n-C_{14}SH to n-C_{16}SH monolayers can probably be ascribed to the fact that monolayers with the length above C_{14} are essentially rigid, while those with the length equal or less than C_{14} are fluid. Thus,

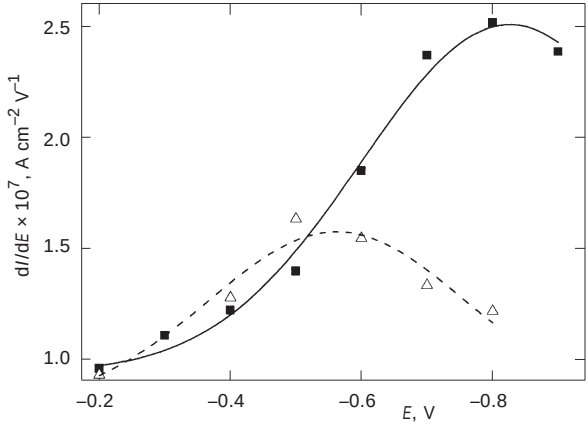

FIG. 4
Plots of dI/dE values *vs* E, obtained by differentiating the I *vs* E curves in Fig. 3, in the case of n-C_{12}SH- (△) and n-C_{14}SH-coated mercury (■). The lines correspond to the Gaussian fits through the data

alkane-1-thiol monolayers ranging from *n*-C_9SH to *n*-C_{14}SH maintain their impermeable, barrier properties toward inorganic redox couples upon expansion of the supporting mercury drop up to *ca* 30%, thus behaving as continuous, liquid films[26]. Conversely, monolayers with chain lengths above *n*-C_{14}SH fracture upon drop expansion in excess of about 5%, thus behaving as essentially rigid films. This abrupt passage from a liquid to a rigid state at room temperature is also revealed by an abrupt increase in the resistance of the thiol film. Table I summarizes values of resistance *R* and capacity *C* of the four alkane-1-thiol monolayers employed, as determined by impedance spectroscopy. It is known that the resistance of an alkane-1-thiol monolayer is much more sensitive to the film compactness and ri-

TABLE I
Differential capacity and resistance of alkane-1-thiol monolayers of different chain length

Parameter	*n*-C_{12}SH	*n*-C_{14}SH	*n*-C_{16}SH	*n*-C_{18}SH
C, μF cm^{-2}	1.04	0.88	0.75	0.70
R, MΩ cm^2	0.21	0.48	2.45	2.63

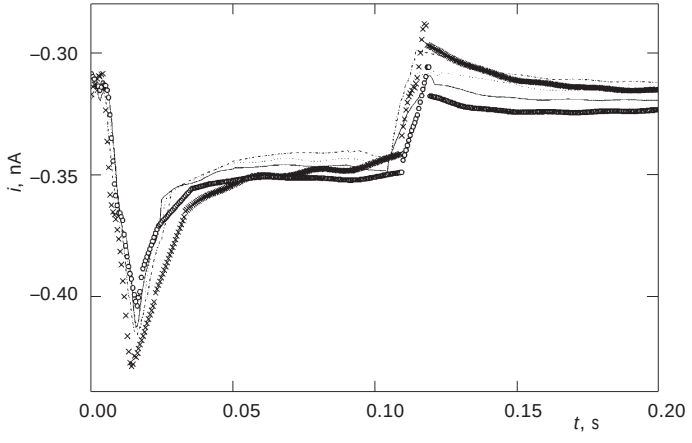

FIG. 5
Light-on and light-off currents recorded upon illuminating a Chl film self-assembled on the top of an *n*-C_{16}SH-coated HMDE in aqueous 1×10^{-1} M KCl (pH 8.5) with red light for 0.11 s at the indicated potentials (in V): –0.3 (×), –0.4 (-·-·-), –0.5 (·····), –0.6 (——), –0.7 (○). Potentials are referred to the Ag|AgCl (1×10^{-1} M KCl) reference electrode. Measurements were carried out on the same freshly prepared drop, starting from the most positive potential and waiting for the stabilization of the background current before illuminating the drop at each potential

gidity than its differential capacity[20]. Thus, the plot of $1/C$ *vs* the thickness of these alkane-1-thiol films is linear, in agreement with the Helmholtz model, and its slope yields a dielectric permittivity of 2, in agreement with the literature[20,26,27].

The fluidity of the *n*-C_{12}SH and *n*-C_{14}SH monolayers may easily allow the intercalation of the Chl phytyl chains within the thiol chains upon Chl self-assembly on the top of the thiol monolayer. In this case electron tunneling will proceed primarily through the phytyl chain covalently bound to the conjugated π-electron system of the porphyrin ring, a pathway that does not change in passing from the *n*-C_{12}SH to the *n*-C_{14}SH monolayer[26]. Probably, the rigidity of the *n*-C_{16}SH and *n*-C_{18}SH monolayers prevents such intercalation, with a resulting notable decrease in the light-on photocurrent. In fact, it was clearly shown that electron tunneling across alkane-1-thiol monolayers proceeds predominantly through σ-bonds of the alkane chains, and only to a small extent through space. Further evidence for this explanation is provided by similar experiments carried out with chlorophyllide, which differs from Chl by the absence of the phytyl chain, where no such abrupt change in behavior is observed on passing from *n*-C_{14}SH to *n*-C_{16}SH monolayers (unpublished results). The decrease in the light-on current in time observed on *n*-C_{16}SH-coated mercury (see Fig. 5) can be tentatively ascribed to a purely chemical reaction bringing Chl* to the ground state. The reaction thus competes with electron tunneling from the metal to Chl* that takes place on this monolayer much more slowly than on monolayers of alkanethiols of shorter chain length. Thus, Chl* might transfer its electron to water upon hydrogen formation, followed by water oxidation to oxygen by the resulting Chl^+ radical cation. In this case, a practically potential-independent steady-state photocurrent would ultimately be attained, as observed in Fig. 5.

In conclusion, an alkanethiol film interposed between the mercury surface and the Chl film decreases the photocurrent with respect to that of a Chl film directly self-assembled on bare mercury. However, such a decrease does not proceed regularly with an increase in the thiol chain length, as distinct from what observed with $[Ru(NH_3)_6]^{3+}$ electroreduction[28]. Rather, an abrupt decrease in current is observed on passing from a *n*-C_{14}SH to a *n*-C_{16}SH monolayer. Chl photocurrents across a monolayer of cetyl alcohol spread on the surface of an amalgamated gold electrode were reported by Khanova and Tarasevich[29]. However, these authors observed no photocurrents of Chl directly deposited on amalgamated gold, in contrast to the results obtained in the present laboratory on mercury drop[21,22].

Effects of Some Anions on the Proton Pumping of Bacteriorhodopsin in Purple Membrane Fragments Adsorbed on a Mercury-Supported Mixed HDT|DOPC Bilayer

It has been established over many years that various anions are able to influence the effectiveness of various biological processes. The order of the effectiveness has generally been found to agree with the so-called Hofmeister series[30] (for a review, see ref.[31]). Although slightly different series have been reported, the effects of some common anions appear to vary in the approximate order F^-, PO_4^{3-}, SO_4^{2-}, CH_3COO^-, Cl^-, Br^-, I^-, CNS^-. It is commonly believed that these effects are indirectly related to the structure of the water molecules surrounding these anions[30–32]. When the Gibbs energy gain, resulting from the orientation of water molecules of the primary hydration sheath of the anion with the hydrogen atoms pointing toward the anion, is comparable with the Gibbs energy loss resulting from the unavoidable decrease in the number of H-bonds between the primary and secondary hydration sheaths, there is no preferential orientation for the hydration molecules[32]. The anions exhibiting this behavior (often characterized by larger radii) are called “chaotropic” or “structure-breaking”. On the other hand, when the Gibbs energy gain, resulting from the alignment of water dipoles of the primary hydration sheath along the direction of the electric field created by the anion, predominates, the anion tends to impose its own order to this sheath[32] and is referred to as “cosmotropic” or “structure-making”. The passage from F^- to CNS^- ion along the above Hofmeister series corresponds to a gradual passage from structure-making to structure-breaking anions.

As a rule, structure-breaking anions exhibit a higher permeability through anion channels because they will give up their water of hydration more readily when passing along a channel[33–35]. For the same reason, structure-breaking anions have a higher tendency to adsorb on the surface of proteins, as they are readily deprived of their hydration sheath on the protein side. This is expected to favor protein unfolding and denaturation, which may explain why structure-breaking anions tend to destabilize soluble proteins, while structure-making ones stabilize them[31,36]. High concentrations of structure-making anions decrease the solubility of proteins in water[31,37,38] (salting-out effect) because, by engaging a high number of water molecules in their hydration sheath, they reduce the number of “free” water molecules available for solubilizing the protein; conversely, structure-breaking ions exert a salting-in effect.

The adsorption of structure-breaking anions on the surface of proteins shifts the local electrostatic potential toward negative values[31]. In the case of integral proteins acting as ion pumps, the effect of anion adsorption depends on the particular charge-translocating step of the pump reaction cycle that is affected by this local negative shift of potential. Thus, it was reported that the effectiveness of anions in slowing down the kinetics of Na^+,K^+-ATPase decreases in the order $ClO_4^- > SCN^- > I^- > NO_3^- > Br^-$, *viz.* in the order of decreasing structure breaking[39]. This was explained by a significant decrease in the affinity of ATP to the enzyme, due to the negative shift in the local electrostatic potential induced by the binding of a structure-breaking anion such as perchlorate to hydrophobic domains on the cytoplasmic face of the protein.

Here we will report the effect of the three sodium salts $NaClO_4$, NaCl and CH_3COONa on the proton pumping activity of bR in PM fragments adsorbed on a mercury-supported HDT/DOPC mixed bilayer. Bacteriorohodopsin is a proton pump present in the PM isolated from *Halobacterium salinarium*, which pumps protons from the intracellular side of the membrane, where the electrochemical potential of protons is lower, to the extracellular side, where it is higher[17,40,41]. The energy required to pump protons is provided by light, which converts the chromophore *all-trans*-retinal, attached to the amino group of a lysine residue as a protonated Schiff base, into the 13-*cis* isomer. This isomerization brings the proton of the Schiff base close to the carboxyl group of an aspartate residue, starting a cyclic sequence of conformational transitions and protonation/deprotonation steps that cause transfer of a proton from the intracellular to the extracellular side. Purple membrane fragments are readily adsorbed on thiol/lipid bilayers supported by mercury[12,14], with the extracellular side turned preferentially towards the metal. Therefore, irradiation of the PM adsorbed on an HDT/DOPC bilayer with green light causes a proton flux from the solution towards the metal side of the purple membrane, which must be compensated by a flux of electrons to the metal surface in the external circuit to keep the applied potential constant. This flux is recorded as a negative capacitive light-on photocurrent. Interrupting the illumination causes a smaller positive capacitive light-off photocurrent.

The typical shape of the PM light-on photocurrent is usually interpreted on the basis of an equivalent circuit in which bR is represented as a current source. The dependence of the photocurrent on time ($I_p(t)$) is expressed *a priori* as a sum of exponentially decaying contributions plus a constant contribution b that represents the stationary current[14,42–44]:

$$(I_p(t)) = \sum_{i=1}^{n} a_i \exp(-t / \tau_i) + b \ . \qquad (3)$$

This expression holds strictly for a sequence of n consecutive irreversible monomolecular transitions. In particular, if each transition is much slower than the preceding one, τ_i is the time constant for the i-th transition and the corresponding amplitude a_i is inversely proportional to τ_i. Figure 6 shows the light-on current *vs* time curves obtained by illuminating the PM fragments adsorbed on a mercury-supported mixed bilayer in contact with a pH 7 buffered solution containing 1 M $NaClO_4$, 1 M NaCl or 1 M CH_3COONa. All these curves are satisfactorily fitted with two exponential terms of Eq. (*3*), yielding two time constants τ_1 and τ_2, and with a zero value of the constant term b. The reciprocals of these time constants measure the corresponding rate constants, k_1 and k_2. Their values (in s^{-1}) are: k_1 = 714 and k_2 = 156 for $NaClO_4$, k_1 = 720 and k_2 = 96 for NaCl, k_1 = 455 and k_2 = 74 for CH_3COONa. Figure 7 shows the light-on current *vs* time curves of PM fragments for increasing concentration, c (in mol dm^{-3}), of CH_3COONa. Fitting these curves with Eq. (*3*) yields the following k_1 and k_2 values (in s^{-1}): k_1 = 555 and k_2 = 93 for c = 0.167, k_1 = 513 and k_2 = 90 for c = 0.36, k_1 = 470 and k_2 = 86 for c = 0.50, k_1 = 450 and k_2 = 74 for c = 1.0. It is

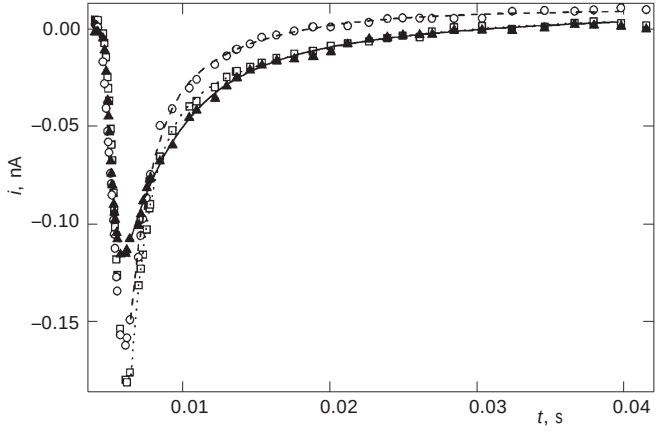

FIG. 6

Light-on currents of PM fragments adsorbed on a mercury-supported HDT/DOPC bilayer, obtained by illumination at E = 0 V *vs* Ag|AgCl (1×10^{-1} M KCl) in aqueous 1 M $NaClO_4$ (○), 1 M NaCl (□) and 1 M CH_3COONa (▲) (all pH 7). Markers are experimental points, while the solid, dashed and dotted curves are best fits to Eq. (*3*). For the parameters employed, see the main text

apparent that a gradual increase in the acetate ion concentration causes a progressive decrease in both rate constants. These rate constants must be ascribed to some step of the bR photocycle.

Upon intense illumination (absorption maximum at 568 nm), bR undergoes a cyclic sequence of transitions between photochemical intermediate states, which are denoted by J, K, L, M (M_1 and M_2), N and O, and are distinguished by their different spectral properties[45,46]. During the first two very fast transitions, the retinal chromophore, attached to the amino group of the lysine 216 residue as a protonated Schiff base, isomerizes from the *all-trans* to the 13-*cis* form, bringing the proton close to the carboxyl group of the Asp-85 residue. During the L to M transition, the proton of the Schiff base is transferred to Asp-85. The protonation of Asp-85 facilitates the deprotonation of a group of neighboring protonated residues, among which probably Glu-204, Glu-194, Arg-82 and several water molecules, called the "proton release complex" (PRC). The latter releases a proton to the extracellular side of the PM[47–49]. During the M to N transition, the Schiff base is reprotonated by Asp-96, which is closer to the cytoplasmic side. In the N state, Asp-96 regains a proton from the cytoplasmic side, while during the concomitant N to O transition retinal isomerizes back from the 13-*cis* to the *all-trans* form. Finally, during the O to bR transition,

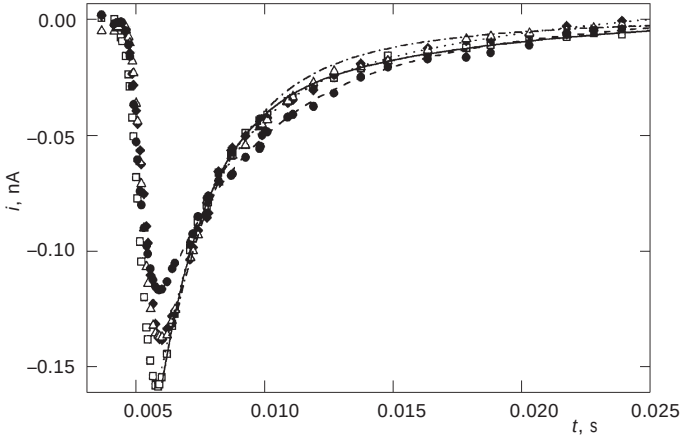

FIG. 7

Light-on currents of PM fragments adsorbed on a mercury-supported HDT/ DOPC bilayer, obtained by illumination at E = 0 V *vs* Ag|AgCl (1×10^{-1} M KCl) in aqueous CH_3COONa (pH 7) of different concentration (in mol dm^{-3}): 1.67×10^{-1} (□), 3.6×10^{-1} (◆), 5×10^{-1} (△) and 1 (●). Markers are experimental points, while the solid, dashed and dotted curves are best fits to Eq. (*3*). For the parameters employed, see the main text

Asp-85 reprotonates the PRC, regaining the initial state and closing the cycle[49,50]. A straightforward assignment of the two rate constants to the steps of the bR photocycle is not possible, since they cannot be directly compared with the "spectroscopic" rate constants available in the literature. In fact, the present rate constants do not necessarily coincide with the "apparent" rate constants obtained from spectroscopic measurements, which are determined from the time constants of the rise and decay of a photochemical intermediate. We can only observe that the apparent rate constant of decay of the O intermediate, determined by Balashov *et al.*[51], decreases from *ca* 100 s^{-1} at pH 6 to 40 s^{-1} at pH 3.0. Thus, it is close to the k_2 value (96 s^{-1}) in 1 M NaCl at pH 7. A similar value of the apparent rate constant was obtained by Li *et al.*[52] in aqueous NaCl. We can, therefore, reasonably ascribe the k_2 values determined herein to the O to bR transition.

The rate constant k_2 increases in the order $CH_3COO^- < Cl^- < ClO_4^-$, which follows the Hofmeister series[30,31]. In fact, acetate is a structure-making ion, perchlorate is a structure-breaking one, while chloride occupies an intermediate position and is often used as a reference. It should be noted that, while the pumping activity of Na^+,K^+-ATPase decreases in passing from structure-making to structure-breaking anions[39], that of bR increases. This behavior can be explained by considering that, when passing from acetate to the more strongly adsorbed perchlorate, the local electrostatic potential at the PRC, which occupies a more peripheral position than Asp-85, may shift in the negative direction; this will cause an acceleration of the O to bR transition, which involves a proton transfer from Asp-85 to the PRC.

In conclusion, while the passage from structure-making to structure-breaking anions along the Hofmeister series is generally characterized by an increase in anion permeability through channels, and by a destabilization and salting-in effect on soluble proteins, the effect of such a passage on ion pumps may be either accelerating or retarding, depending on the nature of the rate-determining electrogenic step of the enzymatic cycle of the pump.

The authors are grateful to Prof. E. Bamberg (Max-Planck-Institut für Biophysik, Frankfurt/Main) for providing them with the purple membrane, and to Prof. A. Agostiano (Department of Chemistry, University of Bari) for providing them with chlorophyll. Bracco S.p.A. and Prof. C. de Häen are gratefully acknowledged for a Ph.D. fellowship of A. Dolfi during the tenure of which some of the present results were obtained. The financial support of the Ministero dell'Istruzione, dell'Università e della Ricerca (MIUR), Italy, and of the Ente Cassa di Risparmio di Firenze are gratefully acknowledged.

REFERENCES

1. Moncelli M. R., Becucci L., Nelson A., Guidelli R.: *Biophys. J.* **1996**, *70*, 2716.
2. Moncelli M. R., Herrero R., Becucci L., Guidelli R.: *Biochim. Biophys. Acta* **1998**, *1364*, 373.
3. Herrero R., Tadini Buoninsegni F., Becucci L., Moncelli M. R.: *J. Electroanal. Chem.* **1998**, *445*, 71.
4. Nelson A., Bizzotto D.: *Langmuir* **1999**, *15*, 7031.
5. Becucci L., Moncelli M. R., Guidelli R.: *Biophys. J.* **2002**, *82*, 852.
6. Lecompte M. F., Miller I. R., Elion J., Benarous R.: *Biochemistry* **1980**, *19*, 3434.
7. Lecompte M. F., Bras A.-C., Dousset N., Portas I., Salvayre R., Ayrault-Jarrier M.: *Biochemistry* **1998**, *37*, 16165.
8. Seifert K., Fendler K., Bamberg E.: *Biophys. J.* **1993**, *64*, 384.
9. Pintschovious J., Fendler K.: *Biophys. J.* **1999**, *76*, 814.
10. Pintschovious J., Fendler K., Bamberg E.: *Biophys. J.* **1999**, *76*, 827.
11. Gropp T., Brustovetsky N., Klingenberg M., Müller V., Fendler K., Bamberg E.: *Biophys. J.* **1999**, *77*, 714.
12. Dolfi A., Tadini Buoninsegni F., Moncelli M. R., Guidelli R.: *Bioelectrochemistry* **2002**, *56*, 151.
13. Dolfi A., Aloisi G., Guidelli R.: *Bioelectrochemistry* **2002**, *57*, 155.
14. Dolfi A., Tadini Buoninsegni F., Moncelli M. R., Guidelli R.: *Langmuir* **2002**, *18*, 6345.
15. Demoz A., Harrison D. J.: *Langmuir* **1993**, *9*, 1046.
16. Brace J. G., Fong F. K., Karweik D. H., Koester V. J., Shepard A., Winograd N.: *J. Am. Chem. Soc.* **1978**, *100*, 5203.
17. Oesterhelt D., Stoeckenius W.: *Methods Enzymol.* **1974**, *31*, 667.
18. Moncelli M. R., Becucci L., Guidelli R.: *Biophys. J.* **1994**, *66*, 1969.
19. Moncelli M. R., L. Becucci L.: *J. Electroanal. Chem.* **1997**, *433*, 91.
20. Tadini Buoninsegni F., Herrero R., Moncelli M. R.: *J. Electroanal. Chem.* **1998**, *452*, 33.
21. Moncelli M. R., Becucci L., Dolfi A., Tadini Buoninsegni F., Agostiano A.: *Bioelectrochemistry* **2002**, *56*, 159.
22. Tadini Buoninsegni F., Becucci L., Moncelli M. R., Agostiano A., Cosma P., Guidelli R.: *J. Electroanal. Chem.* **2003**, *550–551*, 229.
23. Chidsey C. E. D.: *Science* **1991**, *251*, 919.
24. Weber K. S., Creager S. E.: *J. Electroanal. Chem.* **1998**, *458*, 17.
25. Marcus R. A., Sutin N.: *Biochim. Biophys. Acta* **1985**, *811*, 265.
26. Slowinski K., Chamberlain R. V., Miller C. J., Majda M.: *J. Am. Chem. Soc.* **1997**, *119*, 11910.
27. Porter M. D., Bright T. B., Allara D. L., Chidsey C. E. D.: *J. Am. Chem. Soc.* **1987**, *109*, 3559.
28. Slowinski K., Slowinska K. U., Majda M.: *J. Phys. Chem. B* **1999**, *103*, 8544.
29. Khanova L. A., Tarasevich M. R.: *J. Electroanal. Chem.* **1987**, *227*, 115.
30. Hofmeister F.: *Arch. Exp. Pathol. Pharmakol.* **1888**, *24*, 247.
31. Cacace M. G., Landau E. M., Ramsden J. J.: *Q. Rev. Biophys.* **1997**, *30*, 241.
32. Gurney R. W.: *Ionic Processes in Solution*. McGraw–Hill, New York 1953.
33. Bormann J., Hamill O. P., Sakmann B.: *J. Physiol.* **1987**, *385*, 243.
34. Linsdell P., Hanrahan J. W.: *J. Gen. Physiol.* **1998**, *111*, 601.
35. Franciolini F., Nonner W.: *J. Gen. Physiol.* **1987**, *90*, 453.

36. von Hippel P. H., Wong K.-Y.: *Science* **1964**, *145*, 577.
37. Cohn E., Edsall J. T.: *Proteins, Amino Acids and Peptides*. Academic, New York 1943.
38. Green A. A.: *J. Biol. Chem.* **1932**, *95*, 47.
39. Ganea C., Babes A., Lüpfert C., Grell E., Fendler K., Clarke R. J.: *Biophys. J.* **1999**, *77*, 267.
40. Heberle J.: *Biochim. Biophys. Acta* **2000**, *1458*, 135.
41. Brown L. S.: *Biochim. Biophys. Acta* **2000**, *1460*, 49.
42. Borlinghaus R., Apell H.-J., Läuger P.: *J. Membr. Biol.* **1987**, *97*, 161.
43. Fendler K., Jaruschewski S., Hobbs A., Albers W., Froehlich J. P.: *J. Gen. Physiol.* **1993**, *102*, 631.
44. Bamberg E., Apell H.-J., Dencher N. A., Sperling W., Stieve H., Läuger P.: *Biophys. Struct. Mech.* **1979**, *5*, 277.
45. Zimányi L., Váró G., Chang M., Ni B., Needleman R., Lanyi J. K.: *Biochemistry* **1992**, *31*, 8535.
46. Lanyi J. K., Váró G.: *Isr. J. Chem.* **1995**, *35*, 365.
47. Govindjee R., Misra S., Balashov S. P., Ebrey T. G., Crouch R. K., Menick D. R.: *Biophys. J.* **1996**, *71*, 1011.
48. Imasheva E. S., Balashov S. P., Ebrey T. G., Chen N., Crouch R. K., Menick D. R.: *Biophys. J.* **1999**, *77*, 2750.
49. Balashov S. P.: *Biochim. Biophys. Acta* **2000**, *1460*, 75.
50. Luecke H., Schobert B., Richter H. T., Cartailler J. P., Lanyi J. K.: *Science* **1999**, *286*, 255.
51. Balashov S. P., Lu M., Imasheva E. S., Govindjee R., Ebrey T. G., Othersen B., Chen Y., Crouch R. K., Menick D. R.: *Biochemistry* **1999**, *38*, 2026.
52. Li Q., Bressler S., Ovrutsky D., Ottolenghi M., Friedman N., Sheves M.: *Biophys. J.* **2000**, *78*, 354.